CHALMERS
UNIVERSITY OF TECHNOLOGY

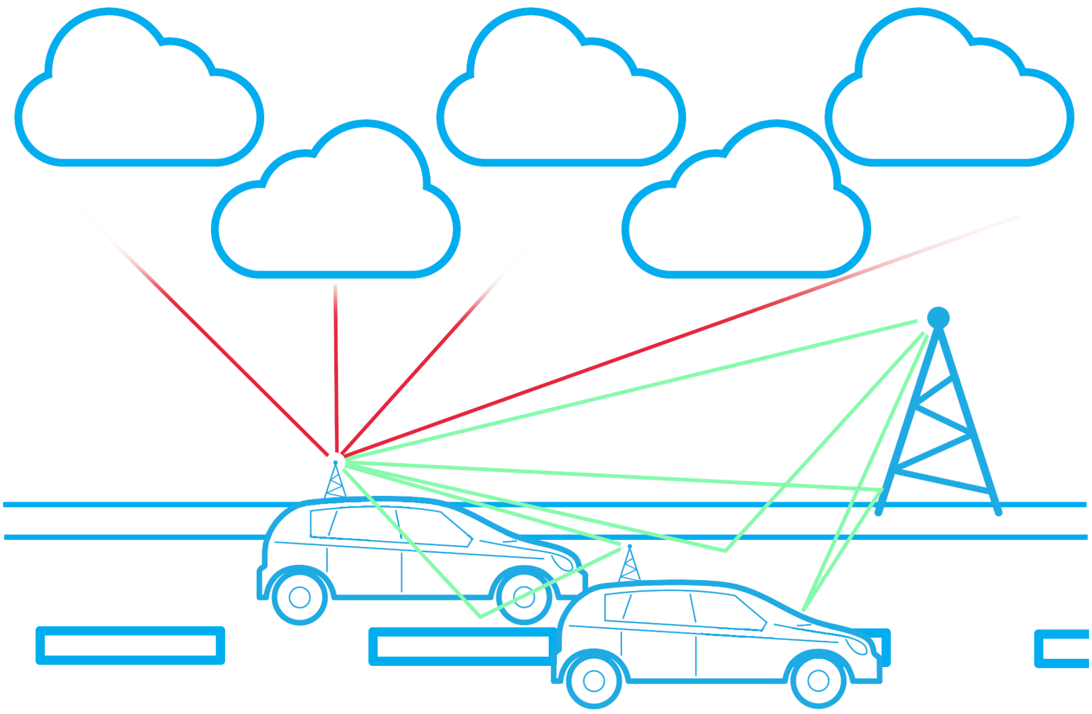

Method for evaluating vehicular antennas in reverberation chambers

Fixture design and construction for emulating non isotropic angle of arrival to sharkfin antennas in reverberation chambers

Master's thesis in Wireless, Photonics and Space Engineering

HENRIK HELMIUS

Department of Electrical Engineering
CHALMERS UNIVERSITY OF TECHNOLOGY
Gothenburg, Sweden 2019

Master's thesis 2019:NN

Method for evaluating vehicular antennas in reverberation chambers

Fixture design and construction for emulating non isotropic angle of arrival to sharkfin antennas in reverberation chambers

HENRIK HELMIUS

Department of Electrical Engineering
Division of Communications, Antennas and Optical Networks
Antenna Systems Group
Chalmers University of Technology
Gothenburg, Sweden 2019

Method for evaluating vehicular antennas in reverberation chambers
Fixture design and construction for emulating non isotropic angle of arrival to shark-fin antennas in reverberation chambers
HENRIK HELMIUS

Supervisor: John Kvarnstrand, Bluetest AB
Examiner: Rob Maaskant, Department of Electrical Engineering

Master's Thesis 2019:NN
Department of Electrical Engineering
Division of Communications, Antennas and Optical Networks
Antenna Systems Group
Chalmers University of Technology
SE-412 96 Gothenburg
Telephone +46 31 772 1000

Cover: Schematic drawing showing the useful radiated energy from a car in green and lost radiation to the sky in red.

Typeset in LaTeX
Printed by [Name of printing company]
Gothenburg, Sweden 2019

Method for evaluating vehicular antennas in reverberation chambers
Fixture design and construction for emulating non isotropic angle of arrival to shark-fin antennas in reverberation chambers
HENRIK HELMIUS
Department of Electrical Engineering
Chalmers University of Technology

Abstract

Previous research shows that elevation angle variations have a large effect on the performance of vehicular antennas. This thesis therefore investigates the non-isotropic properties of communication environments that vehicular antennas experience.

Reverberation chambers are primarily useful for measuring quantities integrated over the whole sphere, such as the antenna radiation efficiency. The isotropic nature of the reverberation chamber fields therefore limits the ability to measure these antennas representatively. A fixture solution for the reverberation chamber, especially aimed at measuring shark-fin antennas, has been proposed. By using microwave absorber mounted above the antenna the aim has been to remove incident radiation above 15° of elevation, effectively only measuring performance close to the horizon. Additionally the fixture was supposed to emulate the effects of a car roof on the antenna performance.

The impact of this fixture has been theoretically investigated. Measurements have been performed on a prototype and the change in radiation efficiency compared to simulated data. Changes in geometry of the prototype have been made to characterize requirements on the design. With optimum geometry these comparisons have shown good agreement, within 0.5dB, for frequencies above 1.5GHz. Antenna patterns with large lobes right above the elevation angle cutoff have however been shown to reduce the performance of the fixture.

Keywords: Reverberation chamber, Sharkfin Antenna, Non Isotropic, Measurements, Vehicular communication, Efficiency.

Acknowledgements

To start of I would like to Bluetest for letting me write my thesis with them. Especially I would like to thank my supervisor John Kvarnstrand for guiding me through the project and giving well needed input when I got stuck.

I would also like to thank the System and Methods team at Bluetest and particularly the S&M Corner answering my stupid questions, helping me in the lab, contributing with design ideas for figures and generally making the workday much more fun.

Additionally I would like to thank Irfan Yousaf at Volvo Cars for lending a shark fin antenna for this project.

Last but not least I would like to thank Emma for supporting me in both the good and the bad as well as taking the time to help me proofread this report.

Henrik Helmius, Gothenburg, December, 2019

Contents

List of Figures

Glossary

AoA Angle of Arrival . . . x
AUT Antenna Under Test . . . 4
DAB Digital Audio Broadcasting . . . 5
DUT Device Under Test . . . 1
GLONASS GLObal NAvigation Satellite System . . . 5
GPS Global Positioning System . . . 5
LOS Line Of Sight . . . xi
LTE Long Term Evolution . . . 5
MEG Mean Effective Gain . . . 11
OTA Over The Air . . . xi
PEC Perfect Electric Conductor . . . 17
RIMP Rich Isotropic Mulitpath . . . 5
PIFA Planar Inverted F Antenna . . . 4
PML Perfectly Matched Layer . . . 17
RC Reverberation Chamber . . . 1
RMS Root Mean Square . . . 24
SDARS Satellite Digital Audio Services . . . 5
TRP Total Radiated Power . . . 19
VNA Vector Network Analyzer . . . 7
WAVE Wireless Acess in Vehicular Environments . . . 5

1
Introduction

A car today is more than a box with an engine and 4 wheels. It's only task is no longer to just transport its passengers from A to B. It's an entertainment device, a navigation device and soon, a driver.

These additional responsibilities we've given the car creates a large need for the car to communicate. Whether it be with a GPS signal, a cellphone tower or other cars. More communication creates a demand for better antennas and to design these, engineers have to be able to test them.

Bluetest manufactures testing equipment for devices based on Reverberation Chamber (RC) technology. The RC can quickly measure the performance of a wireless device isotropically in a fading environment [1].

Isotropic testing can provide representative results for devices used in multiple orientations, therefore requiring good performance no matter the direction from which an incoming signal originates. For a device used in a fixed orientation the incident radiation will however not be isotropic. Most of the energy will enter the antenna at angles close to the horizon, as shown by several previous studies [2]–[4].

A car is an example of just such a device. In most popular use cases all four wheels are in contact with the ground [5], causing the orientation in relation to the ground to remain constant. Fixed on a car an antenna will therefore experience a radiation environment where the AoA is not isotropic, The performance of in the directions of incident radiation thus becomes important.

To representatively measure these it is therefore desirable to modify the behavior of the RC with a higher energy. It can then be used to evaluate a Device Under Test (DUT) for a non uniform distribution of incident radiation.

1.1 Aim of project

The aim of this project has been to design and construct a fixture which can emulate the environment a car mounted antenna will experience in an RC. Specifically this thesis has focused on getting this type of measurement data for sharkfin antennas while also emulating the effects of the roof of a car on which these are usually positioned.

1.2 Layout of thesis

This thesis starts by giving an overview of the background with theory on vehicular communication, channel characteristics surrounding a car and the antennas used. Basic theory on antenna testing in reverberation chambers is then gone through. Afterwards an introduction to the fixture concept is given, followed by a theoretical analysis of its impact.

To get validation data for the performance of the fixture, simulations were performed. This process and the data extraction is described in chapter 5. After that the prototype which was built in order to test the concept is described followed by test results, discussion and a conclusion.

2

Background theory

To motivate the use of the fixture proposed later in this thesis, this chapter presents background information. Both on vehicular wireless technology and measurements in RC.

2.1 Vehicular communication

Vehicular communication shares the same fundamental physics and limitations as all other types of wireless communication. There are however some application specific properties and use cases that influence the design and performance of any device being used for this purpose.

2.1.1 The car environment

In the reference frame of an antenna mounted on a car, the most constant factor is the car itself. It is in a lot of cases built out of metal which will have a large effect on the radiating environment. Most prominently, if the antenna in question is mounted on the roof, a large ground plane will be introduced underneath.

Analytically one can show that if the ground plane is infinitely large it will change the antenna pattern by introducing a virtual image of the antenna beneath the ground plane [6]. Most cars are however not infinitely large and edge effects of the ground plane will therefore contribute to the antenna pattern. This is exemplified by previous research which show that the positioning of an antenna on the roof of a car can have large effects on the realized directivity patterns [7].

2.1.1.1 Channel model

The use of the car in a constant orientation in relation to the ground will cause an antenna mounted on it to maintain an unchanged orientation relative to the horizon. The performance of the antenna will then be affected by the elevation angle characteristics of incident waves in the propagating channel between transmitter and receiver. The elevation angle of a ray in relation to the horizon can be seen in Figure 2.1.

In urban environments the mean elevation AoA has been empirically measured at 3.5GHz to be lower than 15° by Pei et. al.[2]. Their data also suggests that as the

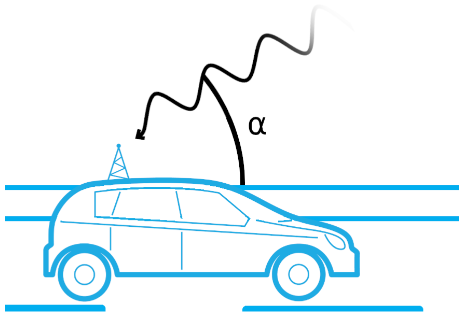

Figure 2.1: Schematic showing the elevation angle α, relative to the horizon, of a ray incident to a car antenna

azimuthal distance between receiver and transmitter increases the average AoA will approach 5°. Pan et. al. [3] have done similar measurements at the same frequency where the mean AoA angle never surpassed 10° for the non LOS case. They also present data for the LOS case with maximum AoA being lower than 20°.

These measurements are accompanied by measurements at 2.15GHz made by Sulonen et al. [4]. Their measurements where done both in an urban environment as well as in a highway setting with both cases showing a 10dB decrease in power for angles larger than about 15°.

This suggests that to perform representative characterization of an Antenna Under Test (AUT) to be used on a car, the performance for angles lower than 15° is the most important.

2.1.1.2 Sharkfin antennas

Sharkfin antennas are a family of roof mounted vehicular antennas. They share a similar form factor allowing them to fit into a shark fin shaped radome. The radome is used in order to reduce the amount of drag produced while the vehicle is moving and to protect the antennas.

To work with different services at several different frequencies the antenna units often contains several independent antennas. The antenna technology used can vary from Planar Inverted F Antennas (PIFAs) [8], sleeve antennas [9], Vivaldi monopoles [10] and dielectric resonators [11], to several different types of novel antenna designs [12]–[16]. Together with these ground based antennas there are often additional satellite communication antennas located in the modules.

2.1.2 Communication standards and frequency ranges

There are multiple different communication standards being used to communicate to and between cars. Although overlapping the different standards can loosely be sorted into three categories; audio broadcasting, navigation and data transfer.

FM radio, in most countries run at between 88 and 108 MHz[17, Appendix A], might be the most common and thought of by everyday people. In some parts of the world has been accompanied or replaced by Digital Audio Broadcasting (DAB) [18]. This standard has been created to enable broadcasting of audio digitally as a replacement for the old analog FM standard and is run at two bands, the old TV band III around 200MHz and in L band around 1460MHz [19].

Audio broadcasts are also in some parts of the world being done via satellite via a standard called Satellite Digital Audio Services (SDARS) [20]. Joining SDARS in the use of satellites are also several standards used for navigation; Global Positioning System (GPS), GLObal NAvigation Satellite System (GLONASS) and Galileo [21].

When it comes to data transmission there are two large applicable communication standards, the traditional Long Term Evolution (LTE) commonly used for mobile phone communication. It provides general data transmission to the rest of the world. To communicate locally with other cars or roadside infrastructure a new standard called Wireless Acess in Vehicular Environments (WAVE), standardized as 802.11p, is used.

The frequencies used for LTE communication varies between different parts of the world with frequency bands defined from $699 - 3800$MHz [22]. WAVE on the other hand is run at a single band, around 5.9MHz [23]. Characterizing antennas for WAVE-communication is of high importance to predict how a device will work because of the high variability in the local environment surrounding the car.

An example of this is a truck passing between two communication partners, shown to cause large dips in the channel gain [24]. Additionally the speeds involved cause the duration under which the channel exists to be short, increasing the demands of a well working radio unit and in turn increasing the need to characterize antenna parameters in a representative way.

2.2 Antenna measurements in reverberation chambers

There are multiple different methods used while measuring antenna performance and characteristics. Bluetests technology is based on using reverberation chambers to emulate a so called Rich Isotropic Mulitpath (RIMP) environment, see Figure 2.2. This section aims to give an understanding of how measurements in a chamber are performed, what they actually measure and how they differ from other measurement methods.

2.2.1 Antenna propagation

With two antennas in free space and only a Line Of Sight component between them the power transmission follows the formula defined by Friis [25], now commonly referred to as the Friis equation. The modern formulation of this is

$$P_r = \frac{G_t G_r \lambda^2}{(4\pi R)^2} P_t \tag{2.1}$$

(a) Outside view of the RTS65 test chamber

(b) The inside of the RTS65 test chamber showing the turntable and plate mode stirrers

Figure 2.2: One of Bluetests reverberation chambers used in wireless OTA testing.

where P_t and P_r are the power transmitted and received respectively. λ is the wavelength and R is the radial distance between the two antennas. G_t and G_r are the gains of the transmitting and receiving antennas respectively.

As there are so few parameters in the equation, an antenna with unknown gain can easily be characterized in an environment such as this. Free space LOS is used while measuring antennas in anechoic chambers, based on this equation. Free space LOS is however very rarely a representative model of the propagation in a realistic environment.

2.2.1.1 The RIMP environment

In a realistic surrounding one has to introduce a number of objects surrounding the propagation path between the two devices. These objects will introduce other paths of propagation by allowing the signal to be reflected in the surrounding objects.

These paths will in most cases be of different lengths and the total signal received will therefore be a combination of signals with different phase. This difference will cause some of them to interfere constructively and some destructively, effectively degrading the signal power [17].

In dense urban environments or while indoors the LOS component can often be blocked by one or several objects. Without the overpowering signal strength of the LOS component the resulting signal strength will vary based on the phase and amplitude difference between the scattered signal components.

Because of the large number of surfaces being able to reflect the signal in such environments the total signal will be a sum of a large number of signals with a random phase. The sums of the in phase complex components of the signal will become normally distributed according to the central limit theorem. This causes the signal magnitude to be Rayleigh distributed [6].

To describe the environment and analyze fixtures subject to this fading and distribution of signals the RIMP environment has been defined. In the RIMP environment the DUT experiences exactly this Rayleigh fading since the "Rich" in the abbreviation is describing a large amount of incoming waves, typically more than 100. The "Isotropic" part of the expression means that the AoA of incoming waves is uniformly distributed over the whole sphere [1].

2.2.2 Reverberation Chamber

One way of emulating the RIMP environment is by use of the Reverberation Chamber, a cavity electrically large enough that many modes can be excited for the tested frequency. By introducing mode stirrers in the chamber one can change the modes excited. This stirring has traditionally been done by moving physical plates around in the chamber or by spinning a metal fan [6]. It has been shown that the distribution of power in a mode stirred chamber follows the Rayleigh fading of the RIMP environment if the LOS path is blocked [26].

Hill has developed a formula for the average transmission between two antennas in this fading environment [27]:

$$\frac{\langle P_r \rangle}{P_t} = \frac{\lambda^3 Q}{16\pi^2 V} \tag{2.2}$$

where $\langle P_r \rangle$ is the average power received by the receiving antenna, P_t is the transmitted power, λ is the wavelength, Q is the Q-factor of the cavity and V is the volume.

This expression assumes lossless antennas but can be rewritten using

$$Q = \frac{f}{\Delta f} \tag{2.3}$$

as done by Kildal [6] to

$$\langle S_{21}^2 \rangle = \frac{c^3 \mu_{rad1} \mu_{rad2}}{16\pi^2 V f^2 \Delta f} \tag{2.4}$$

where $\langle S_{21}^2 \rangle$ is the average power transmission between the two antennas, c is the speed of light, f is the frequency, μ_{rad1} and μ_{rad2} are the efficiencies of the antennas used and Δf is the average mode bandwidth of the chamber.

The mode bandwidth is inversely related to the delay spread τ [28]

$$\Delta f = \frac{1}{\tau}. \tag{2.5}$$

It has been shown that to achieve good measurement precision in a reverberation chamber the mode bandwidth Δf should be kept small, i.e. the Q and τ should be high and therefore the loading of the chamber low [6].

If one then knows the efficiency of one antenna and the delay spread, the efficiency of a second antenna can easily be solved for in (2.4) and becomes a function proportional to the average power transmission. The power transmission can be determined using a Vector Network Analyzer (VNA). By determining it for multiple different modes in the chamber the average gives an estimation for the efficiency of the AUT. Since we know what distribution the signal should follow one can express the accuracy of the measurement as having a standard deviation following

$$\sigma = \frac{1}{\sqrt{N}}, \tag{2.6}$$

where N is the number of independent mode samples. To get within an accuracy of ± 0.5dB the amount of samples needed is $N = 100$ [6].

In the chambers produced by Bluetest the plate mode stirring is complemented by placing the DUT on a turntable thereby moving it around in the chamber while performing measurements, introducing what's called platform stirring. This has been shown to improve the accuracy of the measurement by increasing the amount of samples [29]. Additionally the chambers use polarization stirring, employing chamber antennas with different polarizations shown to improve the polarization balance [30].

2.2.2.1 Rice K-factor

How well a RIMP environment is emulating the Raleigh fading can be expressed using the Rice K factor which Hill [27] defines as:

$$K = \frac{|E_{d\theta}|^2}{2\sigma^2}, \tag{2.7}$$

where $|E_{d\theta}|$ is the magnitude of the theta component of the direct field and σ^2 is the variance of the real and imaginary parts of the stirred field. For a well stirred chamber this fraction should be very low, corresponding to very low LOS component and large spread of the phases of incoming signals to the DUT.

3

Fixture Proposal

To emulate the channel presented in section 2.1.1.1 this thesis proposes a fixture to be used with a DUT in a Reverberation Chamber. The aim of the fixture is to modify the regular RIMP environment of the RC to represent the non isotropic distribution of incident waves for different elevations. It should also provide a good approximation of the roof of the car in order for the new AoA distribution to interact with an antenna pattern as close to the real one as possible.

3.0.1 Ground plane

To make the environment surrounding of the antenna as similar to a car roof as possible a metal surface is proposed to be placed underneath the antenna. The proposal of the ground plane was that it should make antenna measurements with the fixture as representative as possible. This in comparison to the antenna in a working position above a car roof.

3.0.2 Angle of arrival

To emulate the fixed orientation in relation to the ground and the non uniform distribution of incident waves on a device in a real environment the fixture was proposed to consist of an absorbing structure mounted above the DUT. The aim of the absorbing structure to as absorb any wave emerging from an antenna in a direction which in a real world scenario wouldn't reach any communication partner. In order not to increase the loading of the chamber too much the proposed structure should have a metal covering on the outside.

For a given maximum elevation angle of incident wave ϵ, described schematically in Figure 3.2, the absorbing part of the fixture should then be positioned as in Figure 3.1

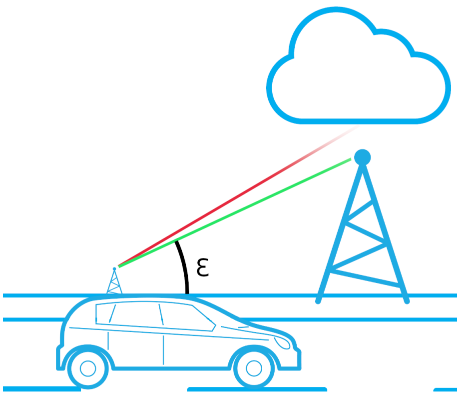

Figure 3.2: Schematic showing ϵ in a LOS environment. ϵ is the largest angle above the horizon for which radiation from a transmitting antenna will encounter a receiving partner.

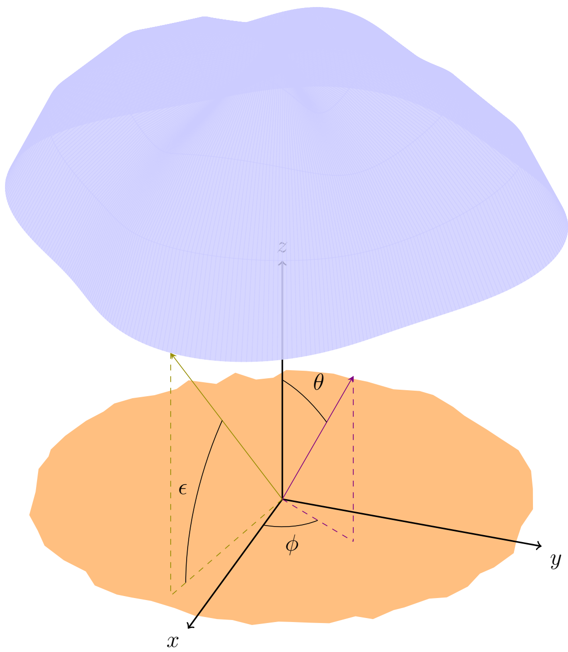

Figure 3.1: The coordinate system of the fixture with the absorbing structure in blue and the ground plane in orange. The traditional spherical coordinate system along with the angle ϵ, the maximum elevation angle of incident waves to be emulated, are also drawn.

3.1 Frequency bands

Since this thesis has focused on simulating a terrestrial environment all satellite based communication standards are disregarded. The workable frequencies in Bluetests RCs are above 450MHz [31]. FM and the lower band used by DAB are below this threshold and have therefore not been of interest in this project. The aim of the proposed fixture is therefore to work on wavelengths used by WAVE and LTE.

4

Theory of fixture impact on RIMP measurements

To understand what is measured with the fixture a theoretical analysis has been performed. The analysis has also been used to help guide design decisions for the fixture and to explain its performance.

4.1 Mean Effective Gain

As defined in section 2.2 the reverberation chamber emulates a Raleigh fading environment. In these environments antennas can be characterized by their Mean Effective Gain (MEG) [6] defined by Taga [32] as:

$$G_e = \frac{P_{rec}}{P_{inc}}. \tag{4.1}$$

Where G_e is the MEG, P_{rec} is the mean received power and P_{inc} is the total mean incident power of the antenna while moving in a multipath environment. To calculate this for a specific antenna in a defined environment Taga specifies the expression:

$$G_e = \int_0^{2\pi} \int_0^{\pi} \left(\frac{XPR}{1+XPR} G_\theta(\theta,\phi) P_\theta(\theta,\phi) + \frac{1}{1+XPR} G_\phi(\theta,\phi) P_\phi(\theta,\phi) \right) sin\theta d\theta d\phi. \tag{4.2}$$

Here XPR is the cross polarization power ratio, G_θ and G_ϕ are the two components of the antenna power gain pattern in θ and ϕ directions, and P_θ and P_ϕ are the probability density functions for incoming plane waves in the θ and ϕ direction. The gain and probability density functions are in these equations normalized as:

$$\int_0^{2\pi} \int_0^{\pi} \left(G_\theta(\theta,\phi) + G_\phi(\theta,\phi) \right) sin\theta d\theta d\phi = 4\pi \tag{4.3}$$

and

$$\int_0^{2\pi} \int_0^{\pi} P_\theta(\theta,\phi) sin\theta d\theta d\phi = \int_0^{2\pi} \int_0^{\pi} P_\phi(\theta,\phi) sin\theta d\theta d\phi = 1. \tag{4.4}$$

Taga does however assume an antenna without any losses. To include an antenna efficiency one can use the definition by Alyon Glazunov et al. [33]

$$\int_0^{2\pi} \int_0^{\pi} \left(G_\theta(\theta,\phi) + G_\phi(\theta,\phi) \right) sin\theta d\theta d\phi = 4\pi \mu_{rad}, \tag{4.5}$$

where μ_{rad} is the radiation efficiency of the antenna.

4.1.1 Mean effective gain in RIMP

In a RIMP environment the AoA is uniformly distributed. This corresponds to

$$P_\theta(\theta,\phi) = P_\phi(\theta,\phi) = \frac{1}{4\pi}, \tag{4.6}$$

in order to comply with the normalization in equation (4.4). If one also assumes that the environment is polarizationally balanced i.e $XPR = 1$ we get

$$G_{eRIMP} = \frac{1}{4\pi}\frac{1}{2}\int_0^{2\pi}\int_0^{\pi} G_\theta(\theta,\phi) + G_\phi(\theta,\phi) sin\theta d\theta d\phi = \frac{\mu_{rad}}{2}, \tag{4.7}$$

using the normalization in (4.5).

4.1.2 Fixture effects

For the case proposed in chapter 3 the environment around the DUT does however not fully emulate a RIMP environment. The proposed semi-RIMP environment changes the probability density functions of the incoming plane waves.

In the simple case where the DUT is located such that the phase center is placed in the center of the fixture this can be expressed analytically. The incident wave distribution becomes uniform over all angles lower than ϵ, the maximum elevation angle of incident waves, defined in chapter 3. For all other angles this distribution becomes 0. In equation form this corresponds to

$$\begin{cases} P_\theta(\theta,\phi) = P_\phi(\theta,\phi) = 0 & \theta < \theta_{app} \\ P_\theta(\theta,\phi) = P_\phi(\theta,\phi) = \frac{1}{2\pi(1-cos(\pi/2+\epsilon))} & \theta \geq \theta_{app} \end{cases}, \tag{4.8}$$

where the fact that the area of a hemisphere on the unit sphere is $2\pi(1 - cos(\alpha))$ has been used. Here the α is the angle from the center axis to the edge. This is required in order to comply with the normalization in equation (4.4).

The limit θ_{app} used here is shorthand for $\pi - \epsilon$, the theta angle corresponding to the top of the aperture. It can be seen as ϵ expressed in the traditional θ-coordinate of the spherical coordinate system, a schematic can be seen in Figure 4.1. It is used in order to simplify the expression while performing spherical integrations. Used in equation (4.2) this distribution of incoming waves gives

$$\hat{G}_e = \frac{1}{2\pi(1 - cos(\pi/2+\epsilon))}\frac{1}{2}\int_0^{2\pi}\int_{\theta_{app}}^{\pi} \left(G_\theta(\theta,\phi) + G_\phi(\theta,\phi)\right) sin\theta d\theta d\phi, \tag{4.9}$$

where $\hat{G}_e$ is the MEG with the fixture. It is important to note that this formula assumes G_θ and G_ϕ defined with the antenna and a ground plane of the same form factor.

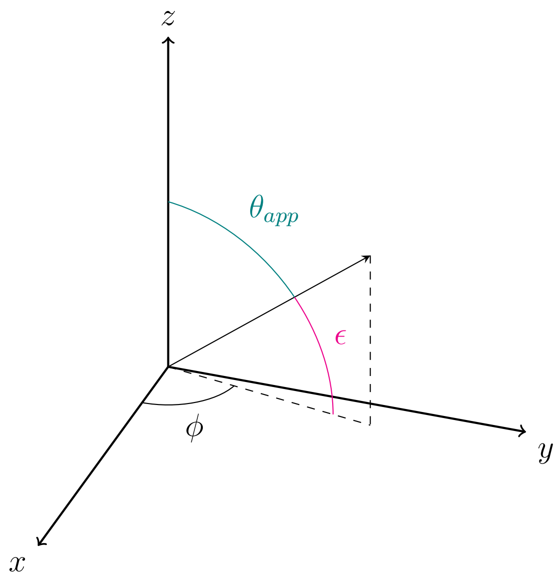

Figure 4.1: Schematic of θ_{app} defined with ϵ

4.2 Radiation efficiency with fixture

If one performs a measurement on the efficiency of an antenna in a RC with the fixture, using the assumption that the efficiency follows the regular RIMP formula (4.7) the apparent efficiency becomes

$$\begin{aligned}\hat{\mu}_{rad} &= 2\hat{G}_e \\ &= \frac{1}{2\pi(1-cos(\pi/2+\epsilon))}\int_0^{2\pi}\int_{\theta_{app}}^{\pi}\left(G_\theta(\theta,\phi)+G_\phi(\theta,\phi)\right)sin\theta d\theta d\phi \\ &= \frac{1}{2\pi(1-cos(\pi/2+\epsilon))}\left(4\pi\mu_{rad}-\int_0^{2\pi}\int_0^{\theta_{app}}\left(G_\theta(\theta,\phi)+G_\phi(\theta,\phi)\right)sin\theta d\theta d\phi\right)\end{aligned} \tag{4.10}$$

where $\hat{\mu}_{rad}$ is the apparent efficiency with the hat. From this we get a formula for the change in efficiency with and without the hat

$$\begin{aligned}\Delta\mu_{rad} &= \frac{\hat{\mu}_{rad}}{\mu_{rad}} \\ &= \frac{1}{(1-cos(\pi/2+\epsilon))}\left(2-\frac{\int_0^{2\pi}\int_0^{\theta_{app}}\left(G_\theta(\theta,\phi)+G_\phi(\theta,\phi)\right)sin\theta d\theta d\phi}{2\pi\mu_{rad}}\right).\end{aligned} \tag{4.11}$$

This will correspond to

$$\Delta\mu_{rad}^{\mathrm{dB}} = \hat{\mu}_{rad}^{\mathrm{dB}} - \mu_{rad}^{\mathrm{dB}} \tag{4.12}$$

in dB-scale.

The change in efficiency of a DUT in a semi-RIMP environment as emulated by the fixture should follow equation (4.11) when compared to without the fixture. It will

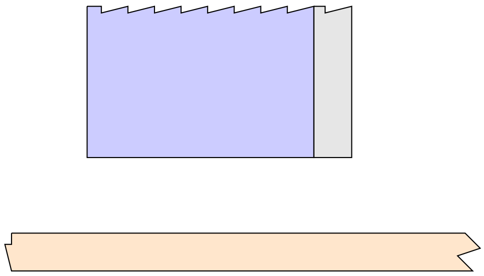

Figure 4.2: Schematic showing a side view of the aperture of the fixture with the absorber, its metal sheathing and the ground plane. The absorber is marked in blue, the ground plane in orange and the metal on the outside in grey.

thus depend on the integral of the gain pattern over the solid angle representing the cutoff area. If this is large, corresponding to a lot of the antennas power being directed to the sky, the efficiency of the antenna in the fixture will be lowered which one would expect.

4.3 Aperture effects

With the roof of the fixture covered in metal and the ground plane extending beyond the outer limits of the absorbing structure a parallel plate waveguide will be created in between the two metal surfaces. This corresponds to the area between the gray and orange fields in Figure 4.2. This waveguide could introduce mismatch producing reflections and frequency dependent behavior.

4.3.1 Cutoff frequency

With a purely vertical polarization of the antenna and no cross polarization the radiating field will have no E or H component in the propagating direction. The field interacting with the parallel plate waveguide will therefore behave as a TEM-wave which in this type of wave guide has no cutoff frequency [34].

If, on the other hand an antenna producing a field with a component in the radial direction is used, the field entering the parallel plate waveguide will not be at TEM-mode it will instead act as a TM-mode which has a cutoff wavelength of $\lambda_c = 2d/n$, where n is the mode number and d is the distance between the two conductors in the waveguide. In our case this distance corresponds to the aperture height between the absorber and the ground plane and will therefore be a function of the radius of the fixture and the sought after ϵ.

4.3.2 Impedance match between inside and outside of the fixture

The introduced parallel plate waveguide will cause an impedance mismatch between the outside free space environment and the parallel plate impedance. This impedance is dependent on the mode excited, TEM, TM or TE. For both TM and TE modes this impedance is only dependent on the height of the waveguide and will approach the free space impedance of 377Ω as this height becomes large [34]. A too small height might however cause an impedance mismatch between the inside and outside of the fixture, giving rise to reflections in the interface between them. The power reflected in the transition will follow the power reflection coefficient

$$|\Gamma|^2 = \left|\frac{Z_L - Z_0}{Z_L + Z_0}\right|^2, \tag{4.13}$$

where $|\Gamma|^2$ is the fraction of power reflected, Z_L is the impedance of the load and Z_0 is the impedance in the original waveguide [35].

The TEM case is a bit more complicated since the theoretical expressions for the impedance is dependent on the width of the waveguide [34]. In the circular case this is hard to define since this becomes the circumference and therefore dependent on the distance from the source. Any change in impedance in this transition will still cause reflections of power following equation (4.13) however.

4.3.3 Propagation between absorber and ground plane

Further in to the fixture, inside the metal edge, a wave propagating between the ground plane and absorber can be thought of as propagating in a partially loaded parallel plate waveguide. Previous research has shown that the propagating solutions for these waveguides are complicated, requiring the introduction of additional boundary conditions in the solving of the wave equation. The impedances of these guides can therefore be hard to calculate analytically, sometimes requiring numerical solving [36]. Their impact on reflections however follows the results predicted by equation (4.13) and a mismatch can therefore give rise to a reduction in radiation flowing out of the fixture.

This part of the propagating path might therefore add additional complications when measurements are being done with the fixture. The fixture should therefore be designed with this in mind and the effects minimized.

4.4 The fixture as a resonator

The covering of the absorbing structure with metal creates a metallic hollow structure. A cavity with a source of microwave energy inside has the potential to become a resonator unless the loading inside is large enough.

From the definition [34]

$$Q = \omega \frac{W_{stored}}{P_{loss}}, \tag{4.14}$$

one can calculate the Q factor of a resonator. Here W_{stored} is the average energy stored and P_{loss} is the energy loss per second. In the case of the fixture the two main loss mechanisms are energy lost in the absorber, $P_{absorber}$ and energy radiated through the aperture $P_{apperture}$.

The difference in impedance between the inside and outside of the fixture, as just examined, could introduce reflections in the interface between them. The loss through the aperture can therefore be written as

$$P_{apperture} = P_{radiated} - P_{reflected}, \tag{4.15}$$

and the Q factor becomes

$$Q = \omega \frac{W_{stored}}{P_{absorber} + P_{radiated} - P_{reflected}}. \tag{4.16}$$

Low absorption in the absorbers in combination with high reflections in the aperture therefore has the potential to give a large Q value and therefore high resonance.

4.5 Intrusion into reactive field

By introducing an absorbing structure electrically close to an antenna one has the risk of affecting the antenna in the reactive near field region. Onishi et. al. have shown that absorbers close to an antenna will affect the efficiency, showing that a distance greater than 0.5λ is required in order to achieve 100% efficiency [37]. This measured 0.5λ distance for good performance is also introduced as a requirement on the distance to walls and metallic stirrers while measuring antennas in a reverberation chamber [6].

The goal when using the fixture is not to change the efficiency of the antenna by introducing absorbers in the near field. The change in efficiency is instead supposed to be representative of a change in the far field of the antenna. Care then has to be taken into when designing the fixture in order to not disturb the near field. Results measured might otherwise not be representative of the environment which is supposed to be emulated here.

4.6 Loading of the chamber

By introducing a large absorbing structure in the reverberation chamber, it can easily be argued that the loss of the chamber will increase. This will in turn lower the Q factor of the chamber. Coating the outside of the absorbing structure with metal should reduce this effect. Some unwanted loss from rays entering the fixture will however most likely occur.

By equation (2.3) this will affect the mode bandwidth experienced in the chamber, possibly reducing the precision of the measurements and because of the inverse relationship decrease the delay spread. Controlling the delay spread in a reverberation chamber has also been shown to be important for certain types of measurements [38]. A decrease in the minimum delay spread might therefore limit the types of measurements which can be performed with the suggested fixture.

5

Simulation of validation data

Detailed data for antenna gain patterns of antennas above ground and over a large frequency band is hard to find. In order to get a reference value for what $\Delta\mu_{rad}$ of an optimally working fixture would produce simulations were therefore run. The results from these were then to be used in order to validate how well the fixture was operating.

5.1 Simulation setup

The simulations where done in the simulation software COMSOL Multiphysics® using the RF physics module. The simulation included the antenna used in the chamber experiments and a ground plane and was implemented as a 2D-axisymetric simulation. This allows one to only model one half of the cross section of a rotationally symmetric model, significantly speeding up the simulations.

This type of simulation is however limited to only simulating objects with a symmetry around a center axis, limiting the possible geometry of the antennas simulated. I have therefore chosen to limit the simulations performed during this thesis to straight wire monopole antennas of different lengths. These antennas fulfill the axisymetric criteria, are easily to manufacture of different lengths and are vertically polarized which makes them operate in a similar fashion to the shark fin antennas.

These antennas, along with the ground plane on which they were simulated got defined in the simulation model as Perfect Electric Conductor (PEC). They were simulated in air which in the far field was terminated by a Perfectly Matched Layer (PML). The excitation of the antenna was done using a lumped port and and the geometry can be seen in Figure 5.1

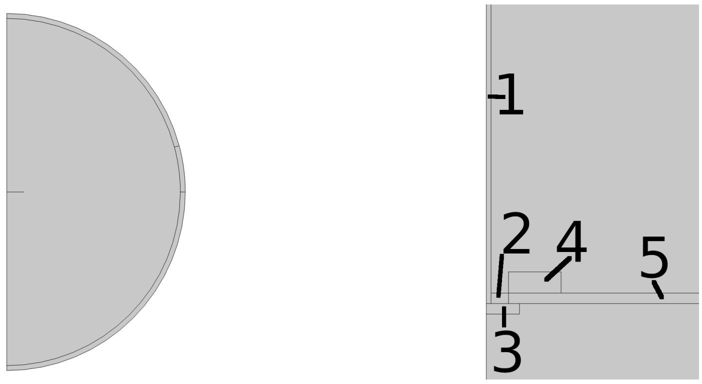

(a) Overview of the simulation setup showing the PML, far away from the ground plane on which the antenna was mounted

(b) Close up of the antenna simulation with parts marked. 1: Antenna, 2: SMA-dielectric, 3: Non simulated domain, 4: Metal flange, 5: Ground plane

Figure 5.1: Figures showing the simulation setup

5.2 Extracting $\Delta\mu_{rad}$

Since the power transmitted from an antenna is directly proportional to the efficiency the simulated power flow from antenna was used in order to calculate a simulated $\Delta\mu_{rad}$.

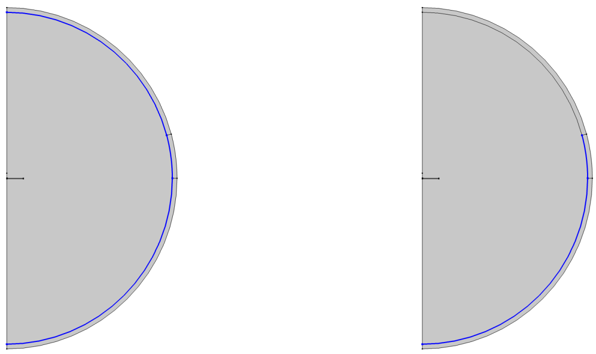

(a) The area over which the integral for P_{TRP} was run

(b) The area used in the integration for P_{ϵ}. In this figure the maximum elevation angle is 15°

Figure 5.2: Blue lines marking the integration areas used in the extraction of the different powers. The line in the middle of the fixture is the ground plane on which the antenna (not visible) was mounted

In COMSOL this was done by extracting the power flow through parts of the edge of the simulation boundary. Figure 5.2 show the surfaces used. The integration over all elevation angles was used as the reference Total Radiated Power (TRP). A different integration, done only over elevation angles lower than ϵ was then run. By dividing the new integration with TRP cancels out any effects by different power transmission and gives

$$\frac{P_\epsilon}{P_{TRP}} = \Delta\mu_{rad}, \tag{5.1}$$

where P_ϵ is the power through all elevation angles lower than ϵ and P_{TRP} is the total radiated power.

The results of this extraction for different variations of the simulated geometry are shown in section 6.3 along with measured values.

6

Prototype construction and measurements

To investigate how well the proposed fixture presented in Chapter 3 works a prototype has been built. Modification of the prototype have been made in order to study their effects and determine requirements on fixture geometry for good results.

The figure of merit first and foremost used in the evaluation is the difference in radiation efficiency of the antenna with and without the absorbing hat. This was defined in equation (4.11) as $\Delta\mu_{rad}$ and should indicate the fraction of power lost to the sky with the antenna in use on a car.

6.1 Prototype

The base configuration of the fixture built to test the fixture idea is shown in Figure 6.1. The structure consists of two circular plates made from plywood. Siepel AH60 foam microwave absorber with a thickness of 6cm has been glued to one side of one of the plates. A cylinder of the same absorbing material has bee glued to the attached absorber in order to create a wall around the perimeter. This microwave absorber is specified to work above a frequency of 1.2GHz. On the outside of the absorbing foam and on the top side of the plywood plate aluminum foil has been glued in order to shield the surfaces.

The other plywood disk has had 4 wooden blocks glued to one side. To these blocks 4 rectangular pieces of plywood have been attached in order to provide support for the hat structure. Additionally 3 metal stand-offs have been attached to the underside of the disk to make it able to attach to the turntable in the RC. One of these stand-offs was made shorter than the other in order to make the fixture sit at an angle. This was done for two reasons: ease of access to the underside of the fixture and a possibility of better mode stirring by making sure the aperture changes direction in the chamber.

The entire non metallic part of this structure has then been covered in aluminum foil which has been glued to the surface. The part of the pillars sticking up from above the ground plane remained uncovered in order to not disturb the radiation pattern of the antenna.

In the base configuration the measurements defined in Figure 6.1 are $r_{gp} = r_{hat} =$ 35cm, $h_{app} = 9.5$cm and $h_{wall} = 15$cm, corresponding to a elevation angle of 15°.

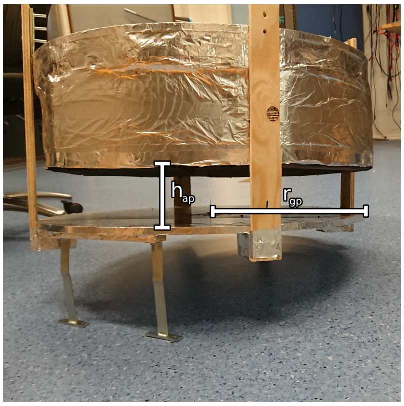

(a) Side view of the fixture showing and defining the aperture height h_{ap} and the ground plane radius r_{gp}

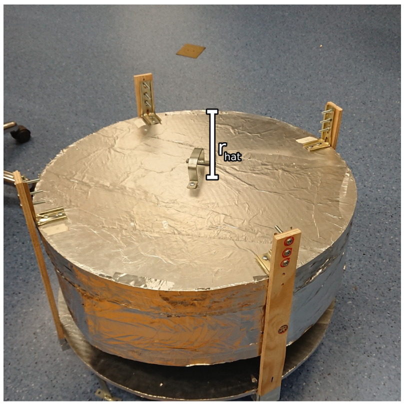

(b) Top view of fixture showing and defining the top radius r_{hat}

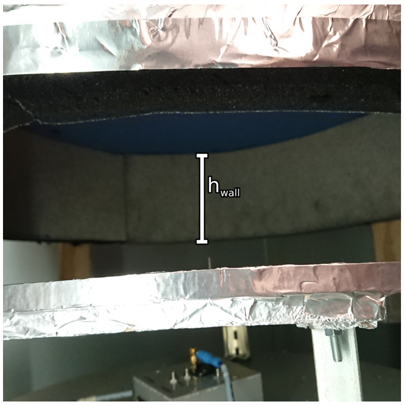

(c) Inside view showing the absorbing structure inside the fixture

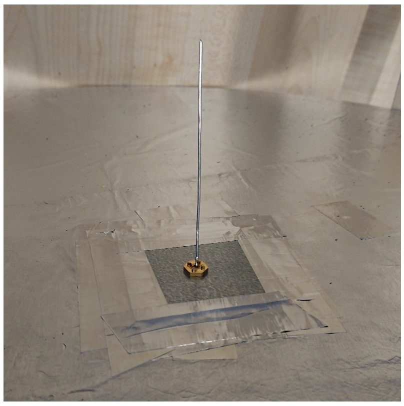

(d) Close up view of the monopole mounted on the ground plane

Figure 6.1: Figures showing the geometry of the built prototype

6.2 Measurement procedure

All reverberation chamber measurements were done in the Bluetest RTS60 reverberation chamber using a Rohde & Schwarz ZNB-8 VNA to acquire the data. The VNA was controlled using the Bluetest Flow software and was calibrated using a Rohde & Schwarz ZV-Z51 automatic calibration unit before every measurement. The calibration was done up to the end of the cable attached to the DUT. In the center of the fixture a quarter wave monopole of varying length was placed. The antenna mounting can be seen in Figure 6.1d.

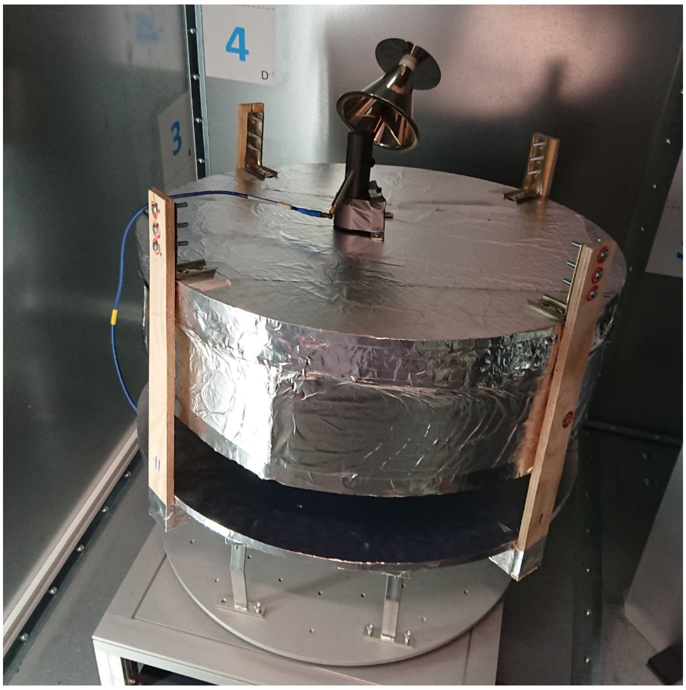

Figure 6.2: Setup for measuring chamber loss with fixture in chamber

6.2.1 Loss

To perform loss measurements in the reverberation chamber a reference antenna with known behavior were used. The reference antenna was placed on the turntable and any item supposed to be included in later measurements was placed in the chamber. Two different reference antennas were used, one for the frequency range 600MHz – 3.5GHz and one for the frequency range 2GHz – 6GHz named discone C and D respectively.

Since the fixture built could not fit in the chamber without standing on the turntable the loss measurements had to be done by attaching the reference antenna to the top of the fixture, see Figure 6.2. Special care was taken to not introduce a LOS component to the signal between the reference and chamber antenna. This was done by inspecting the K-factor, making sure it was low enough.

6.2.2 Efficiency

All efficiency measurements were done using loss measurements of the chamber with the fixture inside as reference. For both the efficiency measurements and their corresponding loss measurement the fixture was kept in the same configuration. The reference antenna used in the corresponding loss measurements was placed on the floor in the chamber with a matching termination.

In the calculation of $\Delta\mu_{rad}$ all efficiency measurements were compared to μ_{rad} for the fixture with the same size ground plane but without the absorbing hat measured in the same way. The loss measurements for these measurements where done without the fixture being mounted on the turntable since there was space for the fixture.

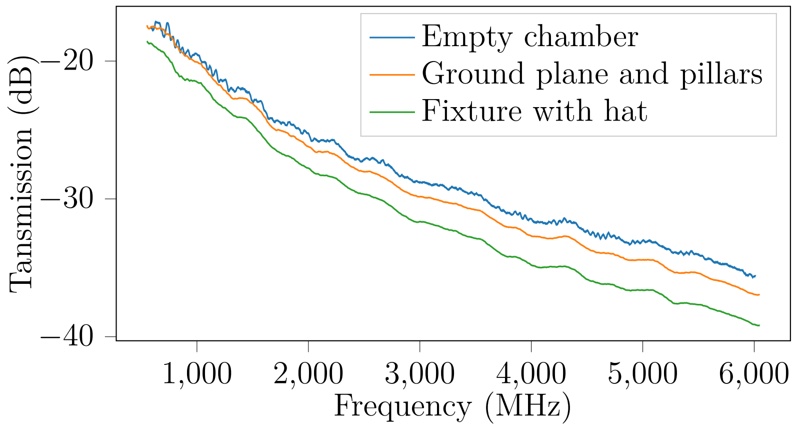

Figure 6.3: The loss of the chamber with and without the base configuration of the fixture

6.3 Results

6.3.1 Loss and loading of chamber

Since the loss of a RC affects the Q value of the chamber and that in turn affects the environment the antenna experiences in it was deemed important to characterize how the fixture effects the transmission in the chamber.

6.3.1.1 Base configuration

The change in loss from the fixture can be seen in Figure 6.3. In the figure three measurements are shown. These correspond to the loss with the empty chamber, the loss with the fixture with absorbing hat and the loss with just the ground plane and support pillars. As we can see, the ground plane it self, without the absorbing structure increases the loss by about 1.2dB at the highest frequency when the loss is highest. The hat then adds an additional 2.4dB to that loss.

The extra loading from this configuration of the chamber resulted in a Root Mean Square (RMS) value for the delay spread of 122.24ns. An empty chamber had the delay spread measured to 130.21ns, a difference of 8ns. Measurements were also done after the ground plane radius was reduced as in Figure 6.15. With the absorbing hat above this ground plane the delay spread was measured to be 97.93ns. Thus lowering the Q factor of the chamber significantly.

6.3.2 Measuring $\Delta\mu_{rad}$

Simulations have given a theoretical reference $\Delta\mu_{rad}$. The fixture under different conditions and configurations has shown different measured $\Delta\mu_{rad}$. By comparing these the limitations of the fixture have been investigated.

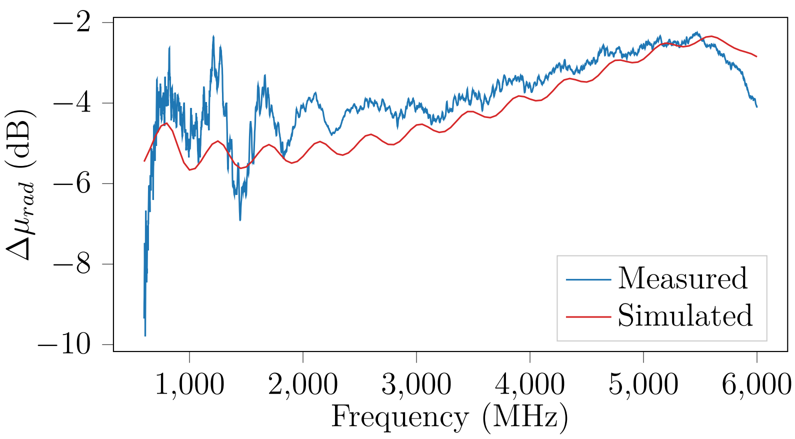

Figure 6.4: The fraction of radiation efficiency measured with the base configuration of the fixture compared to just the ground plane.

6.3.2.1 Base configuration

Efficiency measurements on the base configuration presented in Figure 6.1 with a 3cm long antenna are presented in Figure 6.4. Alongside these the simulated $\Delta\mu_{rad}$ is also plotted. The measured data is a combination of data from the upper and lower frequency ranges as defined by the limitations of the reference antennas. In all plots the data below 3.5GHz uses loss measurements from the C antenna. Data above this uses loss measurements from the D antenna.

As can be seen the fixture produces results within 0.5dB from the reference data for frequencies above 3GHz. One can also see that the periodicity of the simulated $\Delta\mu_{rad}$, corresponding to a wavelength across the diameter of the ground plane, are replicated in measurements.

6.3.2.2 Antenna diagram formation

Changing the length of the monopole antenna while still measuring at the same frequencies has given the opportunity to investigate how well the fixture works for different resonances of the antenna and therefore for different lobe formations.

In Figure 6.5 measured and simulated $\Delta\mu_{rad}$ for a 5.4cm long monopole antenna can be seen. As with the 3cm antenna we see good agreement above 3GHz but as the frequency increases past the resonance at 4.3GHz $\Delta\mu_{rad}$ of the fixture becomes much higher than the simulated. In Figure 6.8a the simulated antenna radiation diagram for this antenna can be seen at 5GHz showing a large lobe directly above an elevation angle of 15°.

Changing the antenna to a longer one with a length of 10.6cm produces the results in figure 6.6. For these measurements the measured results are in very good agreement even under 3GHz where the antenna has a resonance. Above this resonance the behavior seen in the 5.4cm antenna can again be seen, the fixture overestimates $\Delta\mu_{rad}$ for frequencies between 2.2GHz – 3.5GHz. One can again in Figure 6.8b see that the antenna diagram has a large lobe right above 15°.

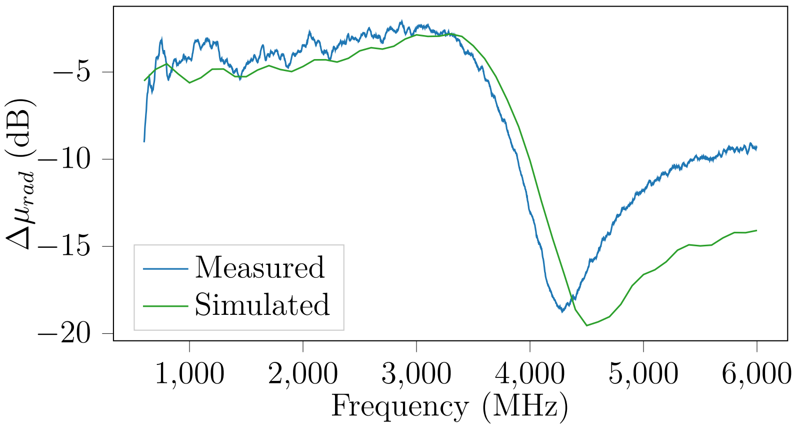

Figure 6.5: $\Delta\mu_{rad}$ for the 5.4cm long antenna

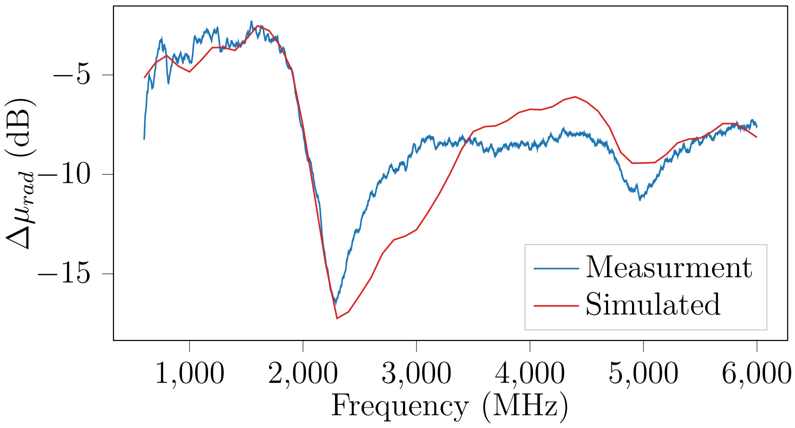

Figure 6.6: $\Delta\mu_{rad}$ for the 10.6cm long antenna

6.3.2.3 Edge diffraction effects

Above 3.5GHz this is no longer the case however, the fixture instead underestimates $\Delta\mu_{rad}$. By computing the simulated value of $\Delta\mu_{rad}$ by using P_{TRP} from a simulation with a ground plane thickness of 1cm and P_{ϵ} from a simulation with a thinner ground plane thickness of 1mm one however gets the results in Figure 6.7.

Disregarding the frequencies for which the antenna main lobe is above the edge of the fixture the simulated and measured $\Delta\mu_{rad}$ follows each other much more closely. This suggests that the antenna acts as though the ground plane has a thickness of 1cm when the hat is not present. But as the absorbing hat of the fixture is introduced the effect of having a thicker ground plane disappears.

The difference in radiation pattern between these two ground planes is most likely coming from double diffraction around the edge with the thicker ground plane. An effect that, according to the measurements seems to go away as the hat is introduced.

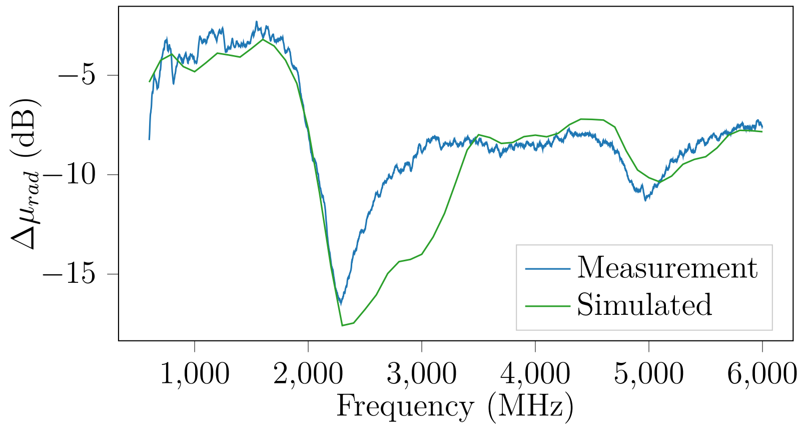

Figure 6.7: $\Delta\mu_{rad}$ for the 10.6cm long antenna where P_{TRP} is simulated with a 1cm thick ground plane and P_ϵ is simulated with a ground plane 1mm thick

6.3.2.4 Correctness with changing ceiling height

In order to investigate how the presence of the absorbing ceiling affects the accuracy of the measurements an additional layer of absorber was added to the ceiling. Assuming total absorption in the absorber this would emulate a fixture where the sidewall height, h_{wall} in Figure 6.1, was lower. The layer was made from the same absorbing material as used in the rest of the fixture. In order to provide more data points that same layer was then moved further down, leaving a gap between it and the absorber glued to the ceiling.

The measurement data from these experiments are presented in Figure 6.9. For all measurements one can observe a large decrease in efficiency below a certain frequency. In this data it can be seen that as the absorber is moved closer to the antenna this frequency increases. For the measured data points the crossover when the efficiency goes above the efficiency of the simulations corresponds to the ceiling being at a distance of 0.5λ away from the antenna.

6.3.2.5 Dependence on distance to absorbing edge wall

By adding additional layers of microwave absorber as can be seen in Figure 6.11 the distance to the absorbing wall from the antenna could be changed which produced the results in Figure 6.10. Adding additional absorber lowers $\Delta\mu_{rad}$ over the entire measured band. The effect of the shorter distance to the antenna seems to become small above 2.5GHz. Change of the radial distance to absorber doesn't seem change the frequency of 3GHz above which the measured and simulated are within 0.5dB of each other.

It is of interest to note that the behavior of the fixture with the highest radius, the unchanged fixture from the base configuration presented in section 6.1, differs somewhat for lower frequencies compared to the results in Figure 6.4. For some frequency points between $1 - 1.5$GHz the difference reaches 2dB. These measurements were performed using the same method and in the same configuration but

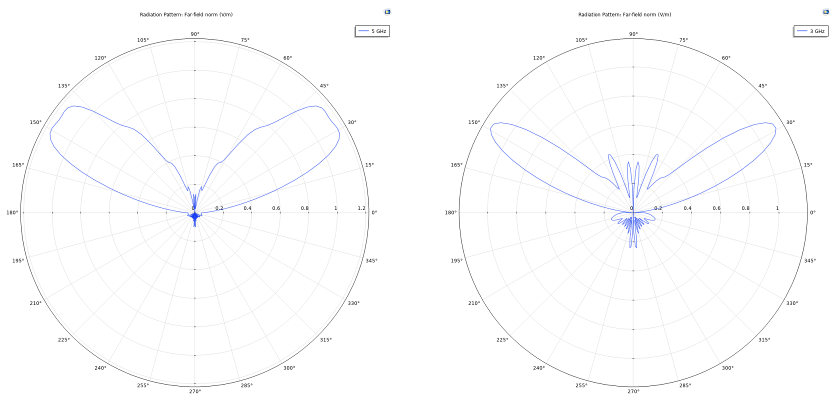

(a) Radiation diagram of the 5.4cm long antenna at 5GHz

(b) Radiation diagram of the 10.6cm long antenna at 3GHz

Figure 6.8: Radiation diagrams for two different monopole antennas above a circular ground plane with a radius of 35cm. Both with a main lobe right above 15°. The radiation diagrams are calculated by COMSOL and are using the simulation model presented in chapter 5.

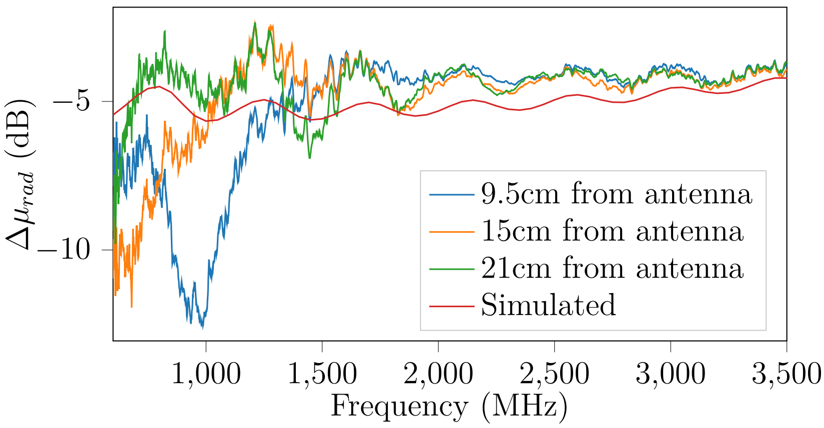

Figure 6.9: $\Delta\mu_{rad}$ for different heights of the ceiling above the antenna

with some other measurements performed in between. This large difference could indicate that the fixture has a certain amount of instability at lower frequencies.

6.3.2.6 Cutoffs frequency investigations by varying aperture height

Section 4.3.1 describes the possibility of introducing cutoff frequencies in the aperture opening. In order to investigate any such effects, measurements where made by changing the height of the hat, H_{ap} in Figure 6.1. H_{ap} was set to 9.5cm, 7cm and 4.5cm corresponding to a maximum allowed incident angle of 15°, 11.3° and 7.3° respectively.

New simulations were made where the new set of elevation angles were used as limits in the calculations of P_{ϵ}. These, along with the measurements on the hat with different heights can be seen in Figure 6.12. This plot shows that the frequency above

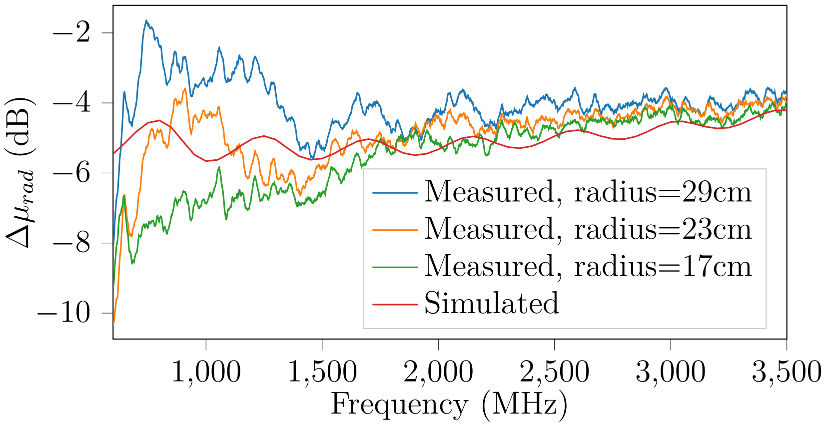

Figure 6.10: $\Delta\mu_{rad}$ for different radial distances from the inner edge of the absorbing wall to the antenna.

Figure 6.11: An additional layer of absorber added to the inside of the edge wall to decrease the inside radius to 46cm. By adding a third layer of absorber to the inside of the layers show the radius could be further reduced.

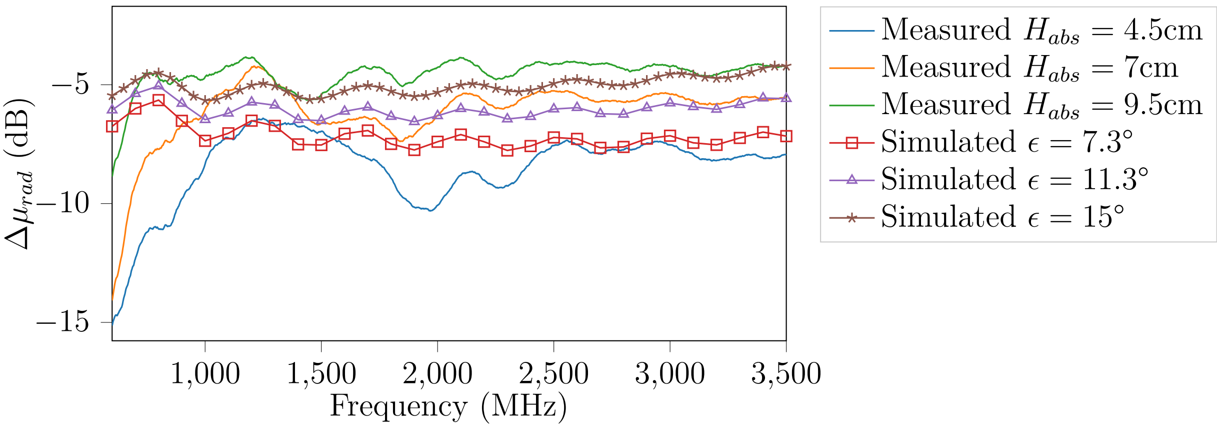

Figure 6.12: $\Delta\mu_{rad}$ for different heights of the aperture opening

which the agreement is within 0.5dB between simulated and measured varies very little between the different heights. Suggesting that the aperture size has limited effect on efficiency measurements.

6.3.2.7 Outer metallic cladding effects investigated by changing the absorber radius

The distance from the antenna to the metal on the outside edge of the fixture has been varied. By modifying the fixture and bringing the the sidewall closer this any changes in measured $\Delta\mu_{rad}$ where investigated. The sidewalls where detached from the ceiling and moved in, see Figure 6.13. The then exposed surface of the roof was covered in aluminum foil

This was done twice, giving opportunities to measure with an outside radius of 26cm and 17cm along with the radius of 35cm in the standard configuration. The antenna used was the 3cm long one used in previous measurements.

When the radius was reduced the aperture height was also lowered in order to maintain the same ϵ of 15°

Figure 6.14 shows the results from these measurements. It is of interest to compare these to the measurements in Figure 6.4 where the radius was unchanged from 35cm. In this comparison one can see that both the configuration with radius at 17cm and the one with 26cm seem to perform better than the original configuration for frequencies between $1.5 - 3$dB. With a few exceptions these configurations of the fixture are within 0.5dB of the simulations in this frequency range, a range in which the base configuration does not perform as well.

The difference in $\Delta\mu_{rad}$ is low between the 26cm measurements and the base configurations. There is however a clear offset, seemingly constant over frequency, when comparing them to the 17cm measurements. This occurs even though the ϵ for the fixture was kept constant during all these measurements. Further more, one can observe that the periodic oscillations in the simulations are no longer present in the measured data.

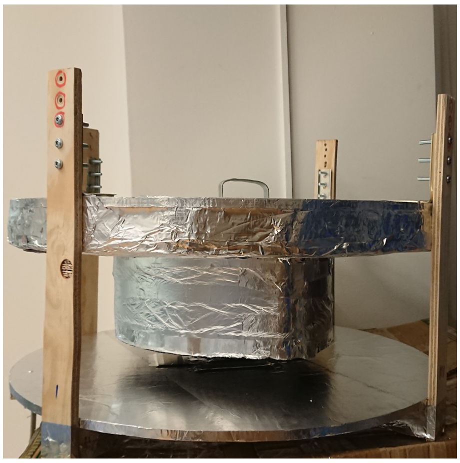

Figure 6.13: Setup of the fixture for measuring with the outside edge closer to the antenna. The outside radius in the picture is 17cm

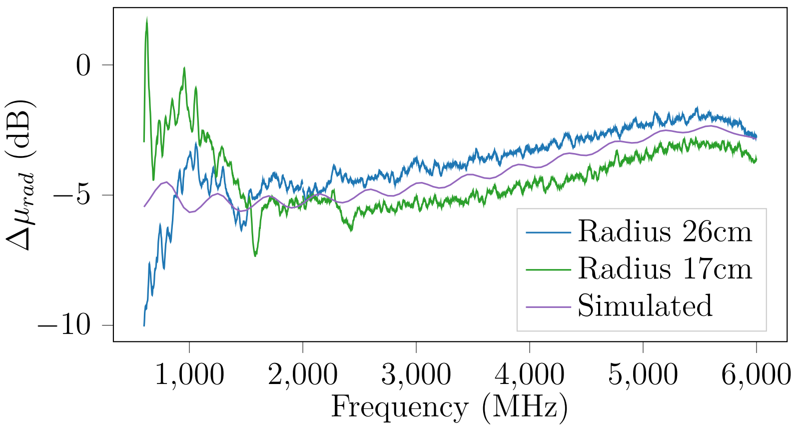

Figure 6.14: $\Delta\mu_{rad}$ when the outside radius was changed.

Figure 6.15: The fixture setup without absorbing hat after the ground plane radius was reduced. Note that the tin foil was removed from any wood part outside the new ground plane edge.

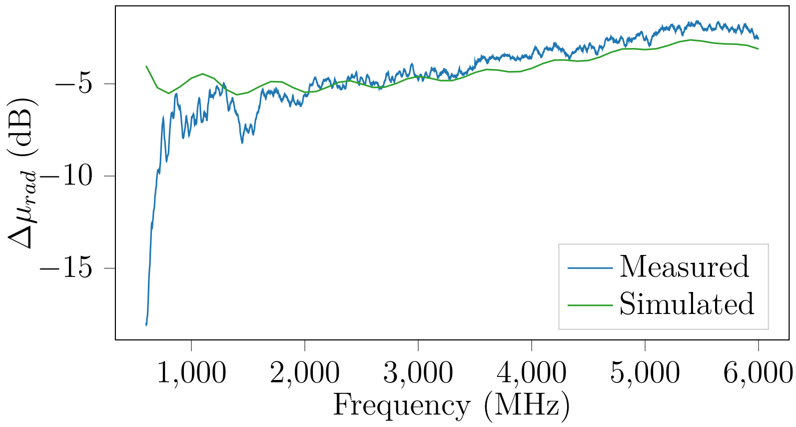

Figure 6.16: $\Delta\mu_{rad}$ when the ground plane radius was reduced to 25cm. The simulations run to produce the values in the graph used a ground plane of the same radius.

6.3.2.8 Impact of varying ground plane size

To investigate the behavior of the fixture with a ground plane smaller than the absorbing hat the ground plane radius was reduced as can be seen in Figure 6.15. The absorbing hat used in these experiments was kept in the same configuration as in the base setup and the aperture height was not changed.

Just as in the case where the outside wall radius was reduced, improved performance for low frequencies can be seen. The measured results are within 0.5dB of the simulated for frequencies above 1.6GHz. Compared to other measurements the results further down in frequency are more stable.

Figure 6.17: Sharkfin antenna supplied by Volvo. The antenna to the left in the image was used in testing.

6.3.3 Measurements on a sharkfin antenna

A shark fin antenna supplied by Volvo, see Figure 6.17, was measured in the fixture. The antenna module contains several antennas however only one of them was measured. During the measurements the other antennas where matched with 50Ω terminations.

The $\Delta\mu_{rad}$ results are seen in Figure 6.18a. As Volvo could not supply any data on performance for multiple elevation angles no validation data exists. One can however evaluate the performance of the DUT. If one disregards the lower frequencies where the hat has not produced very accurate results previously the antenna seems to have a fairly stable lobe formation across the entire frequency range. $\Delta\mu_{rad}$ maintains a value of -4 ± 1dB for most of the frequency range. The only frequency for which this is not the case is surrounding 2.3GHz. Looking at Figure 6.18b it can clearly be seen that this is a frequency for which the antenna is not designed, further confirmed by specifications given by Volvo.

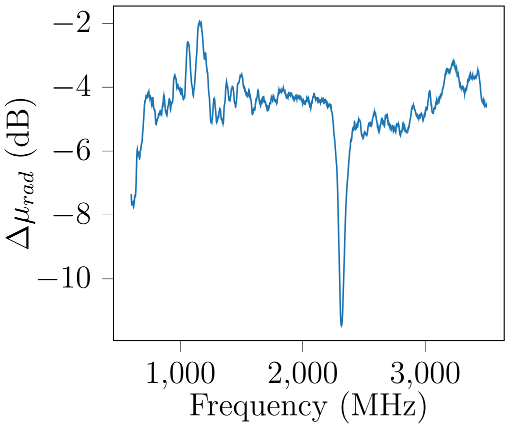

(a) $\Delta\mu_{rad}$ for the sharkfin antenna

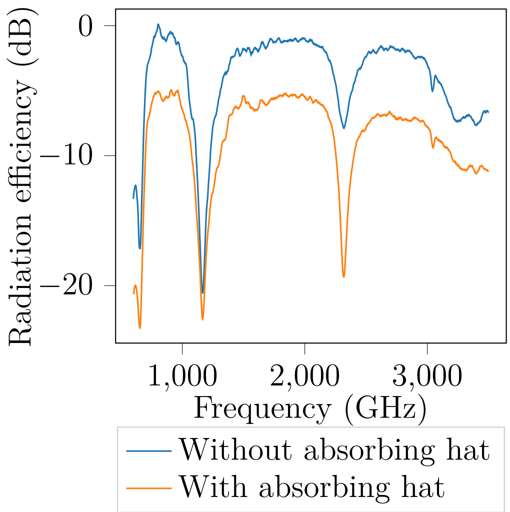

(b) Radiation efficiency of the sharkfin antenna

Figure 6.18: Measurement results from a sharkfin antenna used with the fixture

7

Discussion

Results from the theoretical analysis of the fixture proposal along with simulated and measured results give a basis on which some conclusions can be drawn. These give an indication as to how well the concept works and how a to design a fixture like this for optimal performance.

7.1 Fixture size requirements for optimum performance

Based on the results in section 6.3.2.4 and 6.3.2.5 the effects of absorber intrusion into the reactive field of the antenna are not uniform over elevation angle. The results from measurements when ceiling height was changed indicate that the distance to absorber in the traditional up direction, $\theta = 0$, contributes greatly to the result below 0.5λ away from the antenna.

The distance requirement to the absorber close to the opening of the fixture appears to be higher. In Figure 6.10, $\Delta\mu_{rad}$ for the measurement with the radius being 23cm seems to start following the base measurement closely above 1.7GHz. For the 17cm radius measurements the same thing occurs at 2.25GHz. At these frequencies the distance to the absorbing wall is both 1.3λ, seemingly indicating that, as a rule of thumb, absorbers close to the opening should be at least 1.3λ away from the source in order not to affect the results. Further away than absorbers in the ceiling where a distance of 0.5λ seems to be adequate.

As frequency decreases the wavelength increases. For measurements with good performance at lower frequencies a larger fixture would thus be needed.

7.1.1 Matching in aperture and edge positioning

None of these changes have however shifted the 3GHz limit for the measurements being within 0.5dB of simulations. This limit was however improved greatly, shifting it to 1.6GHz or lower for measurements where the outside edge of the hat and the edge of the ground plane were dislocated from each other. Two methods showed similar behavior, both reducing the radius of the outside wall and reducing the radius of the ground plane.

The proposed reason for these results is that the presence of both the ground plane edge and the aluminum foil on the outside of the fixture creates an impedance mismatch due to diffraction interaction between the two edges.

Differences between the two methods can however be seen below the 0.5dB frequency limit. Smaller ground planes seems to be more stable for lower frequencies with smaller deviations from the simulated performance. Using an absorbing hat larger than the used ground plane could also potentially give an antenna designer more control over the measurements. Edge effects from the antenna being place close to the ceiling edge could in this configuration possibly be emulated. By using larger ground planes than the absorbing fixture, the effect of edges present on a ceiling might not fully be accounted for in a measurement with the fixture.

Another argument for shrinking the ground plane instead of the hat is improvement the angular accuracy. A proposed cause of the shift seen for the smallest hat radius in Figure 6.14 is that a possible shift of the antenna phase center, away from the surface of the ground plane, no longer becomes negligible. This shift causes the antenna reference horizon to be higher, changing the maximum elevation angle let out by the fixture. The larger the absorbing fixture is the smaller such a difference should become.

If however the delay spread and the Q factor of the chamber is important for measurements one might instead decide to use a larger ground plane.

7.2 Accuracy and limitations

For frequencies at which the used geometry of the fixture seems to work well it has been able to measure $\Delta\mu_{rad}$ within 0.5dB from the simulated values. To get results this good does place some restriction son the antenna gain patterns.

The measurements on both the 5.4cm and 10.6cm show that the fixture has a tendency to under estimate $\Delta\mu_{rad}$ for antennas with large lobes right above the edge of the fixture.

For an antenna designer trying to achieve a large antenna lobe close to the ground this could potentially be an issue. If the antenna accidentally has the main lobe slightly shifted upwards the fixture might fail to show this. Causing the user to think that their design is working as planned.

In the current design the fixture should therefore be used for antennas with patterns known to be more isotropic or with large lobes along the horizon.

7.2.1 Delay spread

The delay spread with a ground plane covering the entire bottom of the aperture was measured and seen to be lowered using the fixture. The change was only 8ns in this configurations. With a smaller ground plane the difference was increased significantly, possibly being a limiting factor, depending on the type of measurements performed.

7.3 Limits of this thesis and further investigations

As is usual with a masters thesis not all concepts and variations could be investigated during the time frame of the project. In order to develop this concept into a functioning product there are a still a few design factors which need to be investigated and their impact on the performance characterized.

7.3.1 Further tests with smaller ground planes

The greatly improved behavior seen when moving the ground plane and hat edges away from each other was discovered during the last measurements in the thesis. Scheduling of these experiments to be performed last where motivated by the fact that they required significant remodeling of the fixture. As a precaution, in case of a loss of the fixture, absorber distance, aperture changes and lobe formation investigations were performed ahead of the changes. The values for these experiments presented here are therefore given for a fixture with sub optimal performance.

One area of interest is therefore re-investigating the effects of distance to absorber with smaller ground planes. Partly to confirm whether or not the same phenomena arises and party to get better indications of what the requirements on the fixture are. It would also be of great interest to see if the ground plane thickness changing behavior from section 6.3.2.3 is maintained or disappears in this configuration.

7.3.2 Antenna properties

One type of investigation which has not been done in this thesis is looking at non vertically polarized antennas. Changing the polarization and introducing a horizontal component has the possibility to introduce issues with cutoff frequencies in the aperture between the ground plane and the hat.

Limitations of the 2D axisymetric model used in the simulations have been the cause for this not being done in the current thesis. 3D simulations should be used for this. Because of the size of the fixture and the large frequency band over which this thesis has wanted to investigate this has led to too high simulation times. These are caused because of the small grid size for simulations required at the highest frequencies.

The possibility to measure active antennas with the fixture is also not a topic which has not been investigated, neither theoretically or experimentally.

7.3.3 Ground plane effects

Additionally, in order to fully understand the change in matching in the interaction between the ground plane and the edge of the hat further investigations should be made. By simulating the entire fixture more understanding of the phenomenon could be gained.

Full fixture simulations could also potentially provide with a solution to the inaccuracy of the fixture when antenna lobes close to the edge are used.

7.3.4 Full fixture simulations

A fairly large amount of time in this project has was been spent on trying to model and perform these full fixture simulations. However, these simulations have not produced any representative results compared to real life measurements. The the main issue was thought to be an inability to properly simulate the absorber. Two methods were used while trying to do this.

The first approach was modeling the absorber as a PML which gave unphysical results, sometimes introducing gain. The PML implemented in COMSOL has high reflection while the incidence angle approaches parallel [39]. This is thought to be, at least a partly, the culprit for the problems with this simulation setup since the low ϵ of 15° was used, causing large parts of the fixture to have surfaces almost parallel to any beams. This in combination with being in the very near field of the antenna could cause the problems seen in the simulations.

The second approach was to simulate the absorber as a material with complex permittivity and conductivity. The results from these simulations where more reasonable but representative values of the physical properties of absorbers where hard to find leading to results which did not match measured values. The main issue with getting more accurate values of these parameters has been that manufacturers of absorbers are reluctant to provide them since they are seen as company secrets. I do however think that this approach is the better one for continued research as long as better data can be used in the model.

7.3.5 Differing AoA distributions and non ground plane based antennas

Although some parts of the design are still to be investigated the absorbing structure has shown to be able to emulate the modified non isotropic RIMP. Expanding on the investigations in this thesis further investigations could be done in order to apply this to other types of antennas. The performance observed with smaller ground plane, even though a large absorbing structure is exposed to the chamber, suggest that non isotropic measurements could be performed in the same way on non ground plane based antennas.

Satellite antennas face the inverse problem to sharkfin antennas when mounted on a car. In their use case a low amount of radiated power close to the ground is preferable. Using the same principles as has been presented in this thesis measurements such as this should be able to be performed. Additionally comments in discussions with car manufacturers have suggested that there is a demand for not only having an upper elevation angle limit but also a lower one. Using the current concept this would require additional absorbing structures, possibly introducing new aperture effects needing to be investigated.

8

Conclusion

Based on the results shown in this thesis and the review of literature there is both a need and a potential to perform non isotropic measurements of sharkfin antennas in a reverberation chamber. Using an absorbing structure mounted in the camber, fixed to the antenna, has proven to have the ability to emulate the non isotropic measurements sought after. Some criteria has to be met in order to produce good results.

For good performance with a fixture such as this a distance from the antenna to the structure should be larger than 0.5λ for all directions. Further, closer to the edge of the structure, a distance of 1.3λ should be used for minimum disturbance. Ground planes used should have the edge located a distance away from the structure. For optimum performance and inclusion of edge effects in the results, the ground plane is recommended to be smaller than the absorbing structure unless high delay spreads are required.

With size requirements met, the largest limitation discovered in with the fixture approach is the performance with large antenna lobes just outside the specified solid angle. Further investigations into mitigating these effects are required.

Potential can be seen in the further development of absorbing reverberation chamber fixtures. This development could enable measurements on different types of antennas along with different types of AoA distributions.

Bibliography

[1] P. S. Kildal and J. Carlsson, "New approach to OTA testing: RIMP and pure-LOS reference environments & a hypothesis", in *2013 7th European Conference on Antennas and Propagation, EuCAP 2013*, IEEE, 2013, pp. 315–318.

[2] F. Pei, J. Zhang, and C. Pan, "Elevation Angle Characteristics of Urban Wireless Propagation Environment at 3.5 GHz", in *2013 IEEE 78th Vehicular Technology Conference (VTC Fall)*, IEEE, 2013, pp. 1–5.

[3] C. Pan and J. Zhang, "Experimental investigation of elevation angles and impacts on channel capacity in urban microcell", in *2015 International Conference on Computing, Networking and Communications (ICNC)*, IEEE, 2015, pp. 11–15.

[4] K. Sulonen and P. Vainikainen, "Handset antenna evaluation based on measured distributions", in *IMTC 2001. Proceedings of the 18th IEEE Instrumentation and Measurement Technology Conference. Rediscovering Measurement in the Age of Informatics (Cat. No.01CH 37188)*, vol. 1, IEEE, 2001, pp. 519–524.

[5] J. R. Funk, J. M. Cormier, and S. J. Manoogian, "Comparison of risk factors for cervical spine, head, serious, and fatal injury in rollover crashes", *Accident Analysis & Prevention*, vol. 45, pp. 67–74, 2012.

[6] P.-S. Kildal, *Foundations of Antenna Engineering: A Unified Approach for Line-of-Sight and Multipath*. Kildal Antenn AB, 2015.

[7] E. Whalen, A. Elfrgani, C. Reddy, and R. Rajan, "Antenna Placement Optimization for Vehicle-to-Vehicle Communications", in *2018 IEEE International Symposium on Antennas and Propagation & USNC/URSI National Radio Science Meeting*, IEEE, 2018, pp. 1673–1674.

[8] O.-Y. Kwon, R. Song, and B.-S. Kim, "A Fully Integrated Shark-Fin Antenna for MIMO-LTE, GPS, WLAN, and WAVE Applications", *IEEE Antennas and Wireless Propagation Letters*, vol. 17, no. 4, pp. 600–603, 2018.

[9] Q. Wu, Y. Zhou, and S. Guo, "An L-Sleeve L-Monopole Antenna Fitting a Shark-Fin Module for Vehicular LTE, WLAN, and Car-to-Car Communications", *IEEE Transactions on Vehicular Technology*, vol. 67, no. 8, pp. 7170–7180, 2018.

[10] D. V. Navarro-Méndez, L. F. Carrera-Suárez, E. Antonino-Daviu, M. Ferrando-Bataller, M. Baquero-Escudero, M. Gallo, and D. Zamberlan, "Compact wide-band vivaldi monopole for LTE mobile communications", *IEEE Antennas and Wireless Propagation Letters*, vol. 14, no. Vi, pp. 1068–1071, 2015.

[11] T.-L. Chiu, L. Huitema, O. Pajona, and T. Monediere, "Compact and Multi-band MIMO Dielectric Resonator Antenna for Automotive LTE Communications", *International Journal of Antennas and Propagation*, vol. 2018, pp. 1–15, 2018.

[12] D. V. Navarro-Mendez, L. F. Carrera-Suarez, D. Sanchez-Escuderos, M. Cabedo-Fabres, M. Baquero-Escudero, M. Gallo, and D. Zamberlan, "Wideband Double Monopole for Mobile, WLAN, and C2C Services in Vehicular Applications", *IEEE Antennas and Wireless Propagation Letters*, vol. 16, pp. 16–19, 2017.

[13] N. Guan, H. Tayama, M. Ueyama, Y. Yoshijima, and H. Chiba, "A roof automobile module for LTE-MIMO antennas", in *2015 IEEE-APS Topical Conference on Antennas and Propagation in Wireless Communications (APWC)*, IEEE, 2015, pp. 387–391.

[14] I. Goncharova and S. Lindenmeier, "A high-efficient 3-D Nefer-antenna for LTE communication on a car", *8th European Conference on Antennas and Propagation, EuCAP 2014*, no. EuCAP, pp. 3273–3277, 2014.

[15] A. Friedrich, B. Geck, O. Klemp, and H. Kellermann, "On the design of a 3D LTE antenna for automotive applications based on MID technology", *European Microwave Week 2013, EuMW 2013 - Conference Proceedings; EuMC 2013: 43rd European Microwave Conference*, pp. 640–643, 2013.

[16] M. Cerretelli, V. Tesi, and G. B. Gentili, "Design of a shape-constrained dual-band polygonal monopole for car roof mounting", *IEEE Transactions on Vehicular Technology*, vol. 57, no. 3, pp. 1398–1403, 2008.

[17] D. M. Pozar, *Microwave and RF Design of Wireless Systems*. Wiley, 2002.

[18] R. O. Omslandseter, L. Jiao, and M. A. Haglund, "Field Measurements and Parameter Calibrations of Propagation Model for Digital Audio Broadcasting in Norway", in *2018 IEEE 88th Vehicular Technology Conference (VTC-Fall)*, IEEE, 2018, pp. 1–6.

[19] D. Kresta, L. Polak, and T. Kratochvil, "Coexistence between DVB-S/S2 and DAB systems- A special coexistence scenario", *2017 27th International Conference Radioelektronika, RADIOELEKTRONIKA 2017*, pp. 1–5, 2017.

[20] M. Pannozzo, L. S. Drioli, M. Busa, D. Zamberlan, and E. Toniolo, "State of the art review for automotive satellite antennas", in *2010 5th Advanced Satellite Multimedia Systems Conference and the 11th Signal Processing for Space Communications Workshop*, IEEE, 2010, pp. 355–360.

[21] C. Hoelper and M. Poloskey, "Galileo above - A terrestrial Galileo test environment for vehicular applications: Automotive & rail", in *2010 5th ESA Workshop on Satellite Navigation Technologies and European Workshop on GNSS Signals and Signal Processing (NAVITEC)*, IEEE, 2010, pp. 1–5.

[22] A. Perez, *LTE and LTE Advanced*. John Wiley & Sons, Inc., 2015.

[23] C. Campolo, A. Vinel, A. Molinaro, and Y. Koucheryavy, “Modeling broadcasting in IEEE 802.11p/WAVE vehicular networks”, *IEEE Communications Letters*, vol. 15, no. 2, pp. 199–201, 2011.

[24] D. Vlastaras, T. Abbas, M. Nilsson, R. Whiton, M. Olback, and F. Tufvesson, “Impact of a truck as an obstacle on vehicle-to-vehicle communications in rural and highway scenarios”, in *2014 IEEE 6th International Symposium on Wireless Vehicular Communications (WiVeC 2014)*, IEEE, 2014, pp. 1–6.

[25] H. Friis, “Simple Transmission Formula for radio transmission”, *Proceedings of the IRE and Waves and Electrons*, no. 1, pp. 254–256, 1946.

[26] J. Kostas and B. Boverie, “Statistical model for a mode-stirred chamber”, *IEEE Transactions on Electromagnetic Compatibility*, vol. 33, no. 4, pp. 366–370, 1991.

[27] D. A. Hill, *Electromagnetic Fields in Cavities*. John Wiley & Sons, Inc., 2009.

[28] Y. Li, X. Duan, M. Ma, and B. Jiao, “Studies on the coherence bandwidth of high-frequency vehicular communication system with antenna array”, *Wireless Communications and Mobile Computing*, vol. 11, no. 7, pp. 876–887, 2011.

[29] K. Rosengren, P.-S. Kildal, C. Carlsson, and J. Carlsson, “Characterization of antennas for mobile and wireless terminals by using reverberation chambers: improved accuracy by platform stirring”, in *IEEE Antennas and Propagation Society International Symposium. 2001 Digest. Held in conjunction with: USNC/URSI National Radio Science Meeting (Cat. No.01CH37229)*, vol. 3, IEEE, 2001, pp. 350–353.

[30] P.-S. Kildal and C. Carlsson, “Detection of a polarization imbalance in reverberation chambers and how to remove it by polarization stirring when measuring antenna efficiencies”, *Microwave and Optical Technology Letters*, vol. 34, no. 2, pp. 145–149, 2002.

[31] Bluetest AB, *Reverberation Test Systems RTS*. [Online]. Available: `https://bluetest.se/products/chambers` (visited on 2019-10-28).

[32] T. Taga, “Analysis for mean effective gain of mobile antennas in land mobile radio environments”, *IEEE Transactions on Vehicular Technology*, vol. 39, no. 2, pp. 117–131, 1990.

[33] A. Alayon Glazunov, A. Molisch, and F. Tufvesson, “Mean effective gain of antennas in a wireless channel”, *IET Microwaves, Antennas & Propagation*, vol. 3, no. 2, p. 214, 2009.

[34] D. M. Pozar, *Microwave Engineering*, 4th ed. John Wiley & Sons, Inc., 2011.

[35] K. Kurokawa, “Power Waves and the Scattering Matrix”, *IEEE Transactions on Microwave Theory and Techniques*, vol. 13, no. 2, pp. 194–202, 1965.

[36] L. Young, *Advances in Microwaves*, 1:st ed. Academic Press Inc., 1968.

[37] T. Onishi and K. Ito, “Consideration on the characteristics of antennas close to lossy objects”, in *IEEE Antennas and Propagation Society International Symposium (IEEE Cat. No.02CH37313)*, vol. 1, IEEE, 2002, pp. 440–443.

[38] M. A. Garcia-Fernandez, N. Arsalane, M. Mouhamadou, D. Carsenat, C. Decroze, and T. Monediere, "Analysis of antenna diversity performance dependence on multi-antenna channel delay spread in reverberation chamber", in *2012 6th European Conference on Antennas and Propagation (EUCAP)*, IEEE, 2012, pp. 456–459.

[39] W. Frei, *Using Perfectly Matched Layers and Scattering Boundary Conditions for Wave Electromagnetics Problems*, 2015. [Online]. Available: `https://www.comsol.com/blogs/using-perfectly-matched-layers-and-scattering-boundary-conditions-for-wave-electromagnetics-problems/` (visited on 2019-11-12).